Received: 12 September 2025 | Revised: 2 January 2026 | Accepted: 4 January 2026

DOI: 10.1002/alz.71179

Alzheimer's & Dementia®
THE JOURNAL OF THE ALZHEIMER'S ASSOCIATION

RESEARCH ARTICLE

Targeted blood proteome profiling using NULISAseq identifies a high-performance biomarker panel for Aβ pathology quantification and staging

Wenyue Zheng[1,2] | Yuanbing Jiang[1,2] | Hiu Yi Wong[1,2] | Wan Wa Wong[1,2] | Lily K. W. Cheng[1,2] | Elaine Y. L. Cheng[2] | Bonnie W. Y. Wong[2] | Ronnie M. N. Lo[2] | Siu Ki Leung[2] | Fanny C. Ip[1,2,3] | Jacqueline K. Y. Yuen[4] | Yat Fung Shea[4] | Wai Ming Wong[5] | Chun Keung Shum[5] | Hok Man Wai[6] | Vincent C. T. Mok[7] | Timothy C. Y. Kwok[8] | Kin Y. Mok[1,2,9] | Amanda Heslegrave[9,10] | John Hardy[2,9,10] | Henrik Zetterberg[2,9,10,11,12,13,14,15] | Amy K. Y. Fu[1,2,3,16] | Nancy Y. Ip[1,2,3,16]

[1]Division of Life Science, State Key Laboratory of Nervous System Disorders and Daniel and Mayce Yu Molecular Neuroscience Center, The Hong Kong University of Science and Technology, Hong Kong Special Administrative Region, China

[2]InnoHK Hong Kong Center for Neurodegenerative Diseases, Hong Kong Special Administrative Region, China

[3]Guangdong Provincial Key Laboratory of Brain Science, Disease and Drug Development, HKUST Shenzhen Research Institute, Shenzhen-Hong Kong Institute of Brain Science, Shenzhen, Guangdong, China

[4]Geriatrics Division, Department of Medicine, The University of Hong Kong, Pokfulam, Hong Kong Special Administrative Region, China

[5]Department of Medicine and Geriatrics, Tuen Mun Hospital, New Territories West Cluster, Hospital Authority, Tuen Mun, Hong Kong Special Administrative Region, China

[6]Department of Medicine & Geriatrics, United Christian Hospital, Hospital Authority, Kwun Tong, Hong Kong Special Administrative Region, China

[7]Lau Tat-chuen Research Centre of Brain Degenerative Diseases in Chinese, Gerald Choa Neuroscience Institute, Lui Che Woo Institute of Innovative Medicine, Li Ka Shing Institute of Health Sciences, Division of Neurology, Department of Medicine and Therapeutics, The Chinese University of Hong Kong, Shatin, Hong Kong Special Administrative Region, China

[8]Therese Pei Fong Chow Research Centre for Prevention of Dementia, Division of Geriatrics, Department of Medicine and Therapeutics, The Chinese University of Hong Kong, Shatin, Hong Kong Special Administrative Region, China

[9]Department of Neurodegenerative Disease, Queen Square Institute of Neurology, University College London, London, UK

[10]UK Dementia Research Institute, University College London, London, UK

[11]Department of Psychiatry and Neurochemistry, Institute of Neuroscience and Physiology, Sahlgrenska Academy, The University of Gothenburg, Mölndal, Sweden

[12]Clinical Neurochemistry Laboratory, Sahlgrenska University Hospital, Mölndal, Sweden

[13]Wisconsin Alzheimer's Disease Research Center, University of Wisconsin School of Medicine and Public Health, University of Wisconsin–Madison, Madison, Wisconsin, USA

[14]Department of Pathology and Laboratory Medicine, University of Wisconsin School of Medicine and Public Health, Madison, Wisconsin, USA

[15]Centre for Brain Research, Indian Institute of Science, Bangalore, India

[16]Guangdong-Hong Kong Joint Laboratory for Psychiatric Disorders, Hong Kong Special Administrative Region, China

Wenyue Zheng and Yuanbing Jiang contributed equally to this work.

Correspondence
Nancy Y. Ip, Division of Life Science, State Key Laboratory of Nervous System Disorders, Daniel and Mayce Yu Molecular Neuroscience Center, The Hong Kong University of Science and Technology, Hong Kong Special Administrative Region, China.
Email: boip@ust.hk

Funding information
Research Grants Council of Hong Kong (the Collaborative Research Fund), Grant/Award Number: C6027-19GF; Research Grants Council of Hong Kong (Theme-Based Research Scheme), Grant/Award Number: T13-605/18W; Research Grants Council of Hong Kong (General Research Fund), Grant/Award Numbers: HKUST16103122, HKUST16104624, HKUST16102824; Areas of Excellence Scheme of the University Grants Committee, Grant/Award Number: AoE/M-604/16; InnoHK Innovation and Technology Commission of the Hong Kong Special Administrative Region Government, Grant/Award Number: ITCPD/17-9; SIAT–HKUST Joint Laboratory for Brain Science, Grant/Award Number: JLFS/M-604/24; Guangdong–Hong Kong Joint Laboratory for Psychiatric Disorders, Grant/Award Number: 2023B1212120004

Abstract

INTRODUCTION: While current blood-based biomarkers for Alzheimer's disease (AD) are effective for determining amyloid beta (Aβ) pathology positivity/negativity, they are insufficient for quantifying Aβ plaque deposition.

METHODS: We profiled 325 plasma proteins in a Hong Kong Chinese cohort using the Nucleic Acid Linked Immuno-Sandwich Assay (NULISAseq) platform. We analyzed the dysregulation trajectories of the blood proteome along Aβ pathology progression and used machine learning to develop a biomarker panel to quantify Aβ pathology.

RESULTS: We identified 43 blood proteins correlated with Aβ plaque accumulation and selected 8 proteins to construct a model. This model was strongly correlated with amyloid positron emission tomography Centiloid values ($r = 0.89$), enabling quantification of Aβ deposition and classification of early-stage pathology (area under the curve = 0.93).

DISCUSSION: This study provides a systematic profile of dynamic protein alterations during Aβ pathology progression. Moreover, we developed a biomarker assay that accurately quantifies Aβ pathology, offering a potential tool to facilitate early screening and monitoring of amyloid pathology.

KEYWORDS
Alzheimer's disease, amyloid pathology, amyloid beta quantification, blood biomarkers, disease staging, early detection, machine learning

Highlights

- Nucleic Acid Linked Immuno-Sandwich Assay (NULISAseq) was applied to profile the blood proteome during the development of brain amyloid pathology.
- Different immune and neuronal biological processes exhibit distinct and stage-specific dysregulation patterns during amyloid accumulation.
- A machine learning–based, eight-protein blood biomarker panel was developed to accurately predict the quantitative extent of brain amyloid pathology.
- The eight-protein biomarker assay accurately detects early amyloid accumulation and outperforms prediction based on phosphorylated tau 217 alone.

1 | INTRODUCTION

Alzheimer's disease (AD), the leading cause of dementia,[1] is characterized by two key neuropathological hallmarks: amyloid beta (Aβ) plaques and tau neurofibrillary tangles.[2] Cognitive assessments and biological examinations—particularly evaluation of Aβ pathology—are essential for clinical diagnosis of AD. Amyloid positron emission tomography (PET) imaging is the gold standard for assessing brain Aβ pathology. Its results are usually interpreted as either Aβ positive or Aβ negative based on visual reads, guiding diagnosis and treatment eligibility. However, this binary classification can be challenging if Aβ levels are close to the diagnostic threshold, potentially risking misclassification and delayed intervention.[3]

Continuous quantitative measures based on Aβ PET imaging, such as the Centiloid (CL) scale, offer more objective assessments of progressive Aβ accumulation. The CL scale standardizes Aβ pathology: values < 10 indicate no pathology, while values > 30 indicate established pathology.[4] This continuous approach enables the precise staging of Aβ pathology, offering important clinical implications. It objectively captures early Aβ accumulation in the "intermediate range" (i.e., CL values between cutoffs), indicating evolving pathology and enhancing early diagnosis.[4,5] It also helps monitor disease progression and therapeutic response, which are crucial for timely and effective intervention.[6]

Although reliable, Aβ PET imaging is costly and requires specialized infrastructure, limiting accessibility. Therefore, blood-based biomarkers have emerged as less invasive, more accessible alternatives.[7]

RESEARCH IN CONTEXT

1. **Systematic review**: We conducted a comprehensive literature search on PubMed for all articles published from database inception to Sep 3, 2025, without language restrictions using the following keywords: "Alzheimer's disease," "amyloid-β positron emission tomography," "standardized uptake value ratio" "Centiloid," "blood biomarker," "amyloid," "tau," and "phosphorylated tau." Previous studies demonstrate the feasibility of blood-based protein biomarkers, particularly phosphorylated tau (p-tau) proteins, for the binary classification of amyloid beta (Aβ) pathology as positive/negative. However, growing evidence indicates that quantitative measures of Aβ pathology are valuable for precise disease staging and monitoring pathological changes. Current blood biomarkers are inadequate for this quantitative assessment, limiting their clinical utility for early detection, tracking pathological progression, and guiding timely therapeutic intervention. Therefore, there is an urgent need for blood-based biomarkers that can indicate the quantitative extent of Aβ pathology, enabling more accurate, accessible, and efficient assessment of the amount of brain Aβ plaques.
2. **Interpretation**: This study provides the first systematic profile of blood proteomic alterations along Aβ accumulation. We identified novel blood biomarkers associated with Aβ pathology and delineated their complex, dynamic trajectories. Through co-regulation and network analysis, we revealed that these biomarkers represent diverse biological processes, including synaptic transmission, immune response, and extracellular matrix organization, and exhibit distinct dysregulation patterns during Aβ pathology progression. Using machine learning, we developed a panel of eight blood protein biomarkers that capture the heterogeneous dysregulation trajectories. We further constructed a prediction model based on this panel that accurately predicts quantitative Aβ pathology and sensitively detects early Aβ accumulation. This model outperforms p-tau217 and p-tau231 for assessing nuanced Aβ level changes. Thus, this model is a powerful, accessible tool that advances early diagnosis, patient stratification, and precision medicine for Alzheimer's disease (AD).
3. **Future directions**: Our study underscores the value of profiling the blood proteome during continuous Aβ accumulation to discover biomarkers that reflect progressive pathological changes, thereby enhancing the precision of blood-based staging. These findings support the development of high-performance blood assays for quantifying Aβ pathology and monitoring its changes over time, which would be invaluable for clinical trials and practice, especially for Aβ-targeting therapies. Furthermore, these novel biomarkers, which are involved in multiple biological pathways with distinct dynamics, enable a more refined and comprehensive evaluation of the AD pathological continuum, potentially facilitating personalized treatment strategies. Future research will focus on validating the dynamics of these biomarkers and integrating this holistic assessment into clinical workflows, which could transform the risk prediction, diagnosis, and management of AD, paving the way for innovative therapeutic approaches.

Key AD blood biomarkers include Aβ42/40 ratio, phosphorylated tau species (p-tau; e.g., p-tau217, p-tau231, and p-tau181), and NfL (neurofilament light chain)—collectively termed the ATN biomarkers.[8] These biomarkers, particularly blood p-tau217, show high concordance with Aβ PET imaging in binary classification.[9] Notably, blood p-tau217 is particularly correlated with the later stage of Aβ accumulation, while blood p-tau231 is more strongly correlated with the early stage,[10,11] indicating that different biomarkers may better reflect distinct Aβ pathology stages. Additionally, proteins related to synapse function, immunity, and inflammation are also associated with Aβ pathology,[12] and combining multiple biomarkers to leverage their complementary stage-dependent correlations may enhance diagnostic accuracy.[13] However, further study is required to determine whether blood-based biomarkers or combinations thereof accurately reflect Aβ pathology as well as the CL scale.[14,15]

Novel platforms enable high-throughput quantification of multiple biomarkers. NULISAseq (Nucleic Acid Linked Immuno-Sandwich Assay) is a highly sensitive immunoassay that couples antibody-based detection with next-generation sequencing,[16] allowing accurate, simultaneous measurement of multiple p-tau species and other proteins, making it ideal for AD research.[17–19] Analyzing such complex proteomic datasets requires advanced computational methods. Machine learning, particularly least absolute shrinkage and selection operator (LASSO) models, is increasingly applied in biomarker panel development.[20] These models can select features with the highest predictive value and thereby optimize the biomarker panel.

In this study, we used NULISAseq to reveal dynamic plasma proteomic changes associated with brain Aβ accumulation and applied machine learning to develop a predictive biomarker panel. Specifically, we assessed 325 plasma proteins using the NULISA CNS Disease Panel 120 and Inflammation Panel 250 assays in a Hong Kong Chinese cohort that underwent Aβ PET imaging and CL quantification. We identified 43 proteins exhibiting linear or non-linear correlations with brain Aβ deposition. Functional enrichment analysis revealed that these proteins are involved in synaptic transmission, extracellular matrix regulation, cytokine signaling, and leukocyte migration. We also applied LASSO to identify key proteins for predicting Aβ accumulation, which highlighted eight proteins: p-tau217, p-tau231, and six other AD-associated proteins (i.e., neurotrophin 3 [NTF3], placental growth factor [PGF], secreted protein acidic and rich in cysteine-related modular calcium binding 1 [SMOC1], kallikrein-related peptidase 6 [KLK6], cluster of differentiation 4 [CD4], and periostin [POSTN]). Based on

these eight proteins, we constructed a machine learning model for predicting continuous CL values, termed the"CL predictor," which demonstrated high accuracy (r = 0.89). Importantly, the CL predictor outperformed p-tau217 for predicting both continuous CL values and classifying early Aβ pathology (area under the receiver operating characteristic curve [AUC] = 0.91). Taken together, we comprehensively profiled the dynamics of the plasma proteome along brain Aβ accumulation and developed a highly accurate blood biomarker assay for the early detection, monitoring, and precise staging of Aβ pathology.

2 | METHODS

2.1 | Participant recruitment

We recruited participants from the Hong Kong Chinese population. The cohort comprised 179 Hong Kong Chinese individuals aged ≥ 54 years, including 71 individuals with AD, 12 individuals with non-AD dementia, 62 individuals with mild cognitive impairment (MCI), and 34 cognitively normal control (NC) individuals, who visited the Specialist Outpatient Department of the Prince of Wales Hospital of the Chinese University of Hong Kong (CUHK-PWH), Division of Neurology of CUHK-PWH, the Department of Medicine at Queen Mary Hospital, the Department of Medicine and Geriatrics at Tuen Mun Hospital, or the Department of Medicine and Geriatrics at United Christian Hospital. Participants underwent clinical examination, the Montreal Cognitive Assessment (MoCA),[21] blood collection for the measurement of biomarkers, Aβ PET using [^{11}C]-Pittsburgh compound B (PiB), and neuroimaging by magnetic resonance imaging (MRI).[22] The clinical diagnosis of MCI/dementia was based on a comprehensive clinical evaluation conducted by medical practitioners. Each participant's age, sex, and years of education were recorded. The participants also underwent T1-weighted MRI to quantify brain volumes. All participants or the legal guardians of participants provided written informed consent for study participation and sample collection. This study was approved by the Joint Chinese University of Hong Kong–New Territories East Cluster Clinical Research Ethics Committee at CUHK-PWH, the Institutional Review Board, Hospital Authority (CREC ref. no. 2015.461, KC/KE-22-0107 /ER-2, UW 22-027, CIRB-2023-065-1), and Human and Artefacts Research Ethics Committee (HAREC) at the Hong Kong University of Science and Technology (HREP-2023-0179), and the Human Participants Research Panel of The Hong Kong University of Science and Technology (CRP#180).

2.2 | Imaging acquisition and quantification

T1-weighted structural images were acquired using 3-T MRI scanners. Aβ PET imaging was performed using ^{11}C-PiB PET (Methods S1, S2; Figures S1–S3; Tables S1, S2 in supporting information). All participants were assigned to the $A\beta^{Low}$, $A\beta^{Int}$, or $A\beta^{High}$ group according to their amyloid status on PET irrespective of their cognitive status. Low Aβ pathology on Aβ PET was defined as < 10 CL units, intermediate pathology as 10 to 30 CL units, and high pathology as > 30 CL units.

2.3 | Plasma protein measurement

We analyzed plasma samples using a NULISAseq CNS Disease Panel 120 assay and a NULISAseq Inflammation Panel 250 assay (Alamar Biosciences) on an Alamar ARGO prototype system following established protocols.[17,18] Briefly, we centrifuged thawed plasma at 10,000 × g for 10 minutes to remove particulates followed by incubation with DNA-barcoded capture and detection antibodies. We purified immunocomplexes and generated complementary DNA sequences via ligation of paired antibody barcodes using T4 DNA ligase and a specific DNA ligator sequence. We quantified reporter DNA levels by next-generation sequencing. Sequencing was performed by Novogene Co., Ltd. on an Illumina NovaSeq 6000 platform with a PE150 sequencing kit. Quality control included duplicate sample controls, triplicate inter-plate controls, and duplicate negative controls. We calculated NULISA protein quantification (NPQ) values by normalizing target counts to internal control counts per well followed by normalization to the median inter-plate control counts and $\log_2$ transformation. We calculated fold-changes between experimental groups as $2^{\Delta NPQ}$. The mean coefficients of variation for sample control duplicates were 12.36% and 13.72% across 127 biomarkers in the CNS Disease Panel 120 assay and across 250 biomarkers in the Inflammation Panel 250 assay, respectively. We measured the Aβ42/40 ratio as well as levels of p-tau217, p-tau181, glial fibrillary acidic protein (GFAP), and NfL in 350 µL plasma on a Quanterix HD-X with Quanterix NEUROLOGY 4-PLEX E (Aβ40, Aβ42, GFAP*, Nf-L; 103670), pTau-217 (Simoa ALZpath) Assay (104570), or a pTau-181 Advantage V2.1 kit (104111) where appropriate.

2.4 | Discriminative performance evaluation

We evaluated the accuracy of Aβ PET status classification by calculating AUCs using the auc() function from the R pROC package (v1.18.5).[23] The comparisons included CL > 30 versus CL < 10 as well as CL 10 to 30 versus CL < 10. We assessed differences between receiver operating characteristic (ROC) curves using a DeLong test. We used the pr.curve() function of the PRROC R package (v1.4)[24] to perform precision recall analysis.

2.5 | Associations between proteomics and Aβ PET status

We evaluated the associations between plasma biomarkers and Aβ PET status using linear regression models, adjusting for age, sex, apolipoprotein E (*APOE*) ε4 genotype dose, and years of education. To facilitate comparison of effect sizes, which are reported as standardized β coefficients, we standardized plasma proteomic data by

z score. To profile the trajectories of dysregulated plasma proteins in Aβ PET statuses, we set the level of significance to $|\beta| > 0.25$. We determined the associations between dysregulated plasma proteins and AD-associated endophenotypes by linear regression analysis with the covariates above.

2.6 | Associations between proteomics and Aβ PET CL value

To reveal potential linear and non-linear associations, we visualized the protein trajectories along Aβ PET CL values using a linear regression model and a generalized additive model, respectively. We implemented the linear regression model using the lmrob() function of the robustbase R package (v0.99.4.1),[25] adjusting for age, sex, *APOE* ε4 genotype dose, and years of education. We implemented the generalized additive model using the gam() function of the mgcv R package (v1.9.1)[26] with the Gamma (i.e., log-link) model family, adjusting for the same covariates as above. We standardized continuous values by *z* score. We optimized smoothness parameters by comparing the Akaike information criterion (AIC) across γ values from 0.5 to 5. We fit models using restricted maximum likelihood with term selection enabled. We generated partial effect plots for CL associations using the smooth_estimates() function at 100-point intervals and visualized as a z-scored heatmap. We clustered proteins by row using the dist() function of the Stats R package (v4.4.2)[27] and the hclust() function according to the Ward.D2 method. We set the level of significance to effective degrees of freedom (Edf) > 2 and $p < 0.05$. We resolved duplicate proteins across panels by retaining the measurement with the highest Edf. We visualized protein trajectories using locally estimated scatterplot smoothing (LOESS) regression of protein levels represented by partial effect.

2.7 | Comparison of Aβ-associated proteins between patients' blood and brains

We determined if the Aβ-associated plasma proteins were present in the proteomic data from human *post mortem* cortical tissues of the Mount Sinai Brain Bank cohort (i.e., the parahippocampal gyrus region, including 3305 and 2205 gene products positively and negatively associated with Aβ, respectively).[28] We then evaluated the changes of their protein levels in association with Aβ plaque mean density in the brains. We performed protein mapping at the gene symbol level.

2.8 | Correlation network analysis

To evaluate pairwise correlations among plasma proteins, we calculated Pearson correlation coefficients (*r*) using the cor() function. To identify clustering patterns, we performed hierarchical agglomerative clustering on the correlation matrix, using the dist() function to establish a Euclidean distance matrix. We subsequently carried out clustering using the hclust() function, using the Ward.D2 method.

2.9 | Predictive modeling analysis

To identify proteomic features associated with Aβ PET CL estimation, we used LASSO regression because of its ability to select a minimal set of predictive features, computational efficiency enabling robust bootstrap resampling, and reduced risk of overfitting. We conducted model training using the caret and glmnet R packages.[29] We applied a nested 10-fold cross-validation procedure to 100 bootstrap samples generated from the feature selection dataset. We used weighted sampling to address the distribution imbalance of Aβ PET CL values. We evaluated each protein based on its recurrence across 100 bootstrap iterations, with each iteration randomly sampling 75% of the full dataset, yielding scores ranging from 0 to 100. To compute probability scores for Aβ PET CL prediction and classification, we integrated proteins identified through this process into multiple machine learning frameworks, including random forest (RF) in the randomForest R package (v4.7–1.2),[30] XGBoost (XGB) in the xgboost R package (v1.7.11.1),[31] support vector machine (SVM) in the e1071 R package (v1.7-16),[32] LASSO, and generalized linear models (GLMs) in the glmnet R package (v4.1-8).[33] We assessed model performance by Spearman correlation analysis and ROC curve evaluation. To assess the contribution of each feature toward the prediction performance, we applied the SHapley Additive exPlanations (SHAP) analysis in the kernelshap R package (v0.7.0)[33] and the shapviz R package (v0.9.7).[34]

2.10 | Statistical analysis and data visualization

We performed all statistical analyses and generated figures using R (version 4.4.2). We used the Wilcoxon rank-sum test to compare continuous variables between two groups. We used Spearman rank correlation to evaluate the strength and direction of the associations between two continuous variables. We set the level of statistical significance for all comparisons at $p < 0.05$ and calculated 95% confidence intervals. We used the ggplot() function of the ggplot2 R package (v3.5.1)[35] to generate box plots, scatter plots, volcano plots, line charts, and bar plots. We used the pheatmap() function of the pheatmap R package (v1.0.12)[36] to generate heatmaps and correlation matrices. We used the ggroc() function of the pROC R package to generate ROC curves.

3 | RESULTS

3.1 | Associations of plasma ATN biomarkers with Aβ pathology in the Hong Kong Chinese population

NULISAseq can simultaneously measure 325 targets, including central nervous system disease biomarkers (e.g., Aβ42/40 ratio, p-tau217,

TABLE 1 Participant characteristics.

Parameter	Aβ PET Centiloid status				p value
	All	<10	10–30	>30	
Sample size (*N*)	179	60	12	107	–
Clinical diagnosis					
NC	34	32	1	1	–
MCI	62	16	5	41	–
AD	71	0	6	65	–
Non-AD dementia	12	12	0	0	–
Age, years; mean (SD)	72.0 (7.2)	70.5 (7.5)	74.0 (7.3)	72.0 (7.0)	0.16
Sex, % female	58.1	53.3	50.0	61.7	0.49
Education, years; mean (SD)	9.0 (4.8)	11.0 (4.5)	6.0 (5.5)	6.0 (4.5)	0.001
MoCA score, mean (SD)	19.0 (7.2)	26.0 (6.2)	19.5 (5.7)	15.0 (5.9)	<0.001
Aβ PET Centiloid, mean (SD)	48.3 (39.4)	−2.8 (5.3)	17.4 (6.1)	69.3 (23.9)	<0.001
APOE ε4 carriers, %	24.2	8.1	25.0	58.7	<0.001

Abbreviations: Aβ, amyloid beta; AD, Alzheimer's disease; *APOE*, apolipoprotein E; MCI, mild cognitive impairment; MoCA, Montreal Cognitive Assessment; NC, normal control; PET, positron emission tomography; SD, standard deviation.

p-tau231, and NfL) and inflammatory biomarkers (e.g., chemokine ligand 2 [CCL2] and chemokine ligand 3 [CXCL3]). We applied this advanced technology to our Hong Kong Chinese cohort (n = 179; Figure S4 in supporting information). We classified participants based on their Aβ pathology status assessed by Aβ PET imaging and CL quantification. This classification resulted in three groups: 60 individuals with no or low Aβ ($A\beta^{Low}$, CL < 10), 12 with intermediate levels of Aβ ($A\beta^{Int}$, CL 10–30), and 107 with high Aβ levels ($A\beta^{High}$, CL > 30; Table 1). As expected, nearly all individuals in the $A\beta^{Int}$ and $A\beta^{High}$ groups (98.3%) were diagnosed with cognitive impairment (i.e., MCI or dementia) compared to 20% in the $A\beta^{Low}$ group.

We first cross-validated NULISAseq-based ATN biomarkers by comparing their levels to those measured by SIMOA assay. Measurements of the three p-tau biomarkers ($r_{p\text{-}tau217} = 0.88$, $r_{p\text{-}tau231} = 0.90$, $r_{p\text{-}tau181} = 0.87$, all $p < 2.2 \times 10^{-16}$) and NfL ($r = 0.87$, $p < 2.2 \times 10^{-16}$) were strongly correlated between the two assay platforms. Meanwhile, the NULISAseq and SIMOA measurements of the Aβ42/40 ratio were weakly correlated ($r = 0.16$, $p = 4.2 \times 10^{-2}$; Figure S5 in supporting information).

Next, we examined the changes of the Aβ42/40 ratio as well as p-tau217, p-tau231, p-tau181, and NfL levels across different stages of brain Aβ pathology (i.e., the $A\beta^{Low}$, $A\beta^{Int}$, and $A\beta^{High}$ groups). Among the five measured ATN biomarkers, only p-tau217 and p-tau231 showed significant dysregulation at both the $A\beta^{Int}$ and $A\beta^{High}$ stages (p-tau217: $d_{Int} = 1.18$, $d_{High} = 2.48$; p-tau231: $d_{Int} = 1.02$, $d_{High} = 2.03$; all $p < 0.05$; Figure 1B, C), suggesting that they are strongly associated with the development of brain amyloid pathology. In comparison, the Aβ42/40 ratio ($d = -0.35$, $p < 0.05$), p-tau181 level ($d = 1.34$, P$p < 0.05$), and NfL level ($d = 0.60$, $p < 0.05$) were only dysregulated in the $A\beta^{High}$ group (Figures 1A, D and S6A in supporting information), suggesting their late involvement during brain amyloid accumulation. These findings are consistent with previous studies of NULISAseq and SIMOA-based ATN biomarkers in populations of European descent.[18,37,38]

Furthermore, we examined the performance of these ATN biomarkers for classifying Aβ pathology status. For distinguishing individuals in the $A\beta^{High}$ group from the $A\beta^{Low}$ group, p-tau217 performed best (AUC = 0.95) followed by p-tau231 (AUC = 0.92) and p-tau181 (AUC = 0.82); meanwhile, both the Aβ42/40 ratio and NfL level showed low accuracy for distinguishing the two groups (Figures 1E, S6B). Notably, for distinguishing between individuals the $A\beta^{Int}$ and $A\beta^{Low}$ groups, only p-tau217 achieved an AUC > 0.8 (AUC = 0.81) and was closely followed by p-tau231 (AUC = 0.79); meanwhile, p-tau181 (AUC = 0.67), the Aβ42/40 ratio (AUC = 0.51), and NfL (AUC = 0.56) all had AUCs < 0.7 (Figures 1F, S6C). This indicates that these blood ATN biomarkers are insufficient for accurately classifying early Aβ deposition. Moreover, only p-tau217 (AUC = 0.81) and p-tau231 (AUC = 0.80) had AUCs > 0.8 for distinguishing between the $A\beta^{Int}$ and $A\beta^{High}$ groups (Figures 1G, S6D), which is still inadequate for staging brain amyloid pathology. Taken together, the NULISAseq data validate the performance of blood-based ATN biomarkers for classifying brain amyloid pathology in the Hong Kong Chinese cohort, with plasma p-tau217 and p-tau231 accurately detecting established Aβ pathology. Nonetheless, none of these existing blood ATN biomarkers demonstrated sufficient performance for classifying or staging early Aβ pathology.

3.2 | Identification of plasma proteomic signatures at early and established stages of Aβ accumulation

In addition to known ATN biomarkers, other blood proteins may be dysregulated upon the development of AD and amyloid pathology, potentially aiding disease classification and assessment of progression.[39,40]

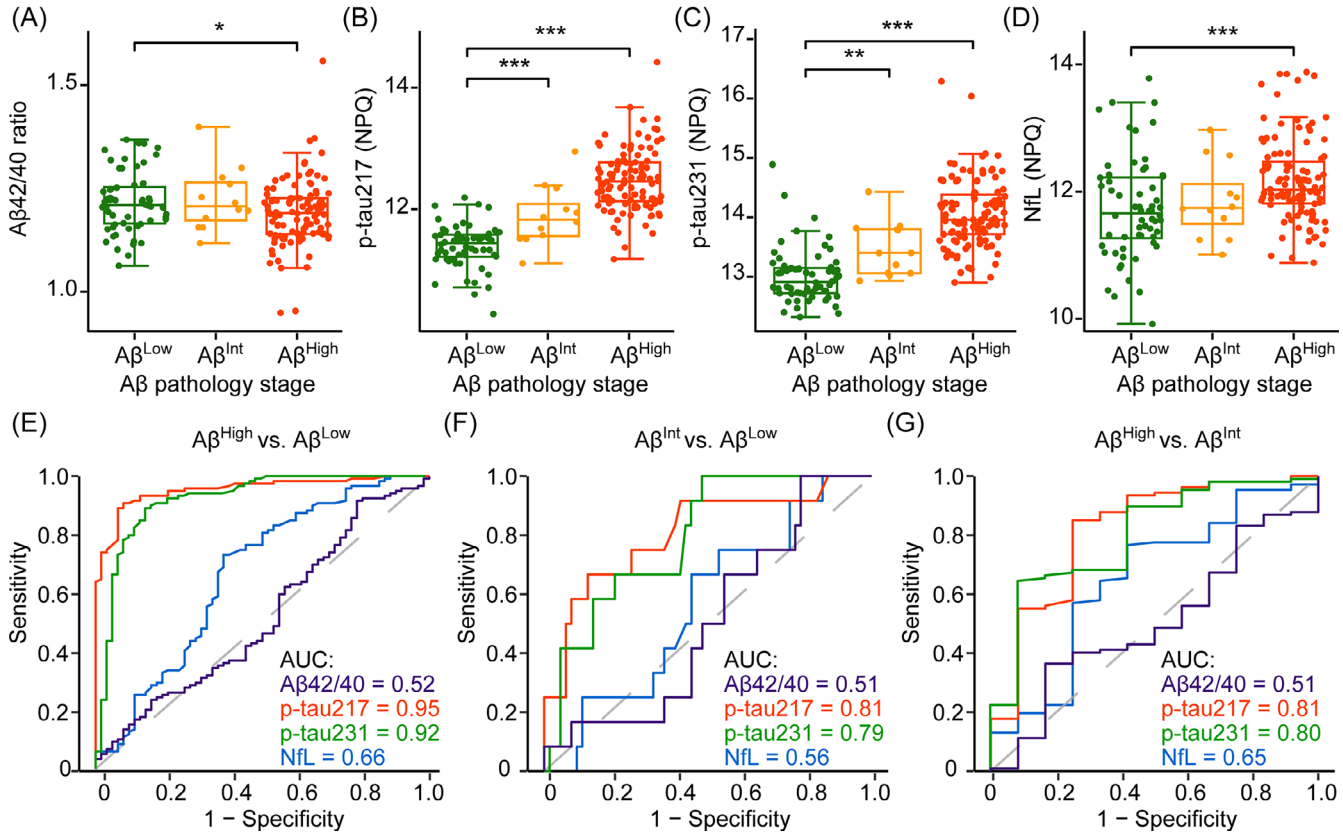

FIGURE 1 Association between plasma ATN biomarkers measured by NULISAseq and Aβ pathology. A–D, Box plots showing the plasma (A) Aβ42/40 ratio, (B) p-tau217 level, (C) p-tau231 level, and (D) NfL level stratified by Aβ pathology status (i.e., $A\beta^{Low}$, CL < 10; $A\beta^{Int}$, CL 10–30; $A\beta^{High}$, CL > 30). A, Aβ42/40 ratio comparison ($d = 0.10$, $p = 0.76$ for $A\beta^{Int}$ vs. $A\beta^{Low}$; $d = -0.35$, $p = 0.03$ for $A\beta^{High}$ vs. $A\beta^{Low}$). B, p-tau217 comparison ($d = 1.18$, $p = 4.64 \times 10^{-3}$ for $A\beta^{Int}$ vs. $A\beta^{Low}$; $d = 2.48$, $p = 2.80\times 10^{-35}$ for $A\beta^{High}$ vs. $A\beta^{Low}$). C, p-tau231 comparison ($d = 1.02$, $p = 5.36\times 10^{-3}$ for $A\beta^{Int}$ vs. $A\beta^{Low}$; $d = 2.03$, $p = 5.17\times 10^{-26}$ for $A\beta^{High}$ vs. $A\beta^{Low}$). D, NfL comparison ($d = 0.18$, $p = 0.53$ for $A\beta^{Int}$ vs. $A\beta^{Low}$; $d = 0.6$, $p = 4.32\times 10^{-4}$ for $A\beta^{High}$ vs. $A\beta^{Low}$). E–G, ROC curves with corresponding AUCs showing the cross-analytical platform comparison of diagnostic performance of the ATN plasma biomarkers for classifying individuals by Aβ pathology status: (E) $A\beta^{High}$ versus $A\beta^{Low}$, (F) $A\beta^{Int}$ versus $A\beta^{Low}$, and (G) $A\beta^{High}$ versus $A\beta^{Int}$. E, Classification of the $A\beta^{High}$ versus $A\beta^{Low}$ groups (Aβ42/40 ratio AUC = 0.52, p-tau217 AUC = 0.95, p-tau231 AUC = 0.92, NfL AUC = 0.66). F, Classification of the $A\beta^{Int}$ versus $A\beta^{Low}$ groups (Aβ42/40 ratio AUC = 0.51, p-tau217 AUC = 0.81, p-tau231 AUC = 0.79, NfL AUC = 0.56). G, Classification of the $A\beta^{High}$ versus $A\beta^{Int}$ groups (Aβ42/40 ratio AUC = 0.51, p-tau217 AUC = 0.81, p-tau231 AUC = 0.80, NfL AUC = 0.65). Wilcoxon rank-sum test; $^{*}p < 0.05$, $^{**}p < 0.01$, $^{***}p < 0.001$. Aβ, amyloid beta; AUC, area under the receiver operating characteristic curve; CL, Centiloid; NfL, neurofilament light chain; NPQ, Nucleic Acid Linked Immuno-Sandwich Assay protein quantified; PET, positron emission tomography; p-tau, phosphorylated tau; ROC, receiver operating characteristic.

We used NULISAseq to screen for novel blood-based protein biomarkers associated with brain amyloid pathology. Specifically, we performed linear regression analysis to determine the associations between each of the 325 assayed protein levels and specific Aβ stages (i.e., $A\beta^{High}$ vs. $A\beta^{Low}$ and $A\beta^{Int}$ vs. $A\beta^{Low}$), adjusting for the effects of age, sex, *APOE ε4* genotype, and years of education. The analysis identified 67 proteins dysregulated in the $A\beta^{High}$ stage ($p < 0.05$), including 19 upregulated and 48 downregulated proteins. Among the 20 proteins that passed false discovery rate (FDR) correction (i.e., FDR < 0.05), the top upregulated proteins included p-tau231, p-tau217, and GFAP, while the top downregulated proteins included agrin (AGRN), SMOC1, and p-SNCA129 (Figure 2A and Table S3 in supporting information). We also examined the blood proteomic changes in early Aβ pathology (i.e., the $A\beta^{Int}$ stage) and identified 60 proteins that exhibited significant dysregulation ($p < 0.05$), including 6 upregulated and 54 downregulated blood proteins (Figure 2B and Table S4 in supporting information). Interestingly, only 27 blood proteins were significantly dysregulated in both the $A\beta^{High}$ and $A\beta^{Int}$ stages compared to the $A\beta^{Low}$ stage, including p-tau217 and p-tau231, and were consistently dysregulated throughout brain amyloid pathology development (Figure S7, Table S5 in supporting information). In comparison, several blood proteins, such as ubiquitin, exhibited opposite dysregulation patterns in the $A\beta^{High}$ and $A\beta^{Int}$ stages (i.e., being upregulated in the $A\beta^{Int}$ stage and downregulated in the $A\beta^{High}$ stage). These findings indicate that the dysregulation of the blood proteome exhibits complex, stage-specific patterns during brain Aβ accumulation.

We subsequently categorized all 100 blood proteins dysregulated in either the $A\beta^{Int}$ or $A\beta^{High}$ stage into five groups based on their dysregulation patterns (Figures 2C and S8; Table S6 in supporting information). Accordingly, 12 proteins (e.g., p-tau217 and p-tau231)

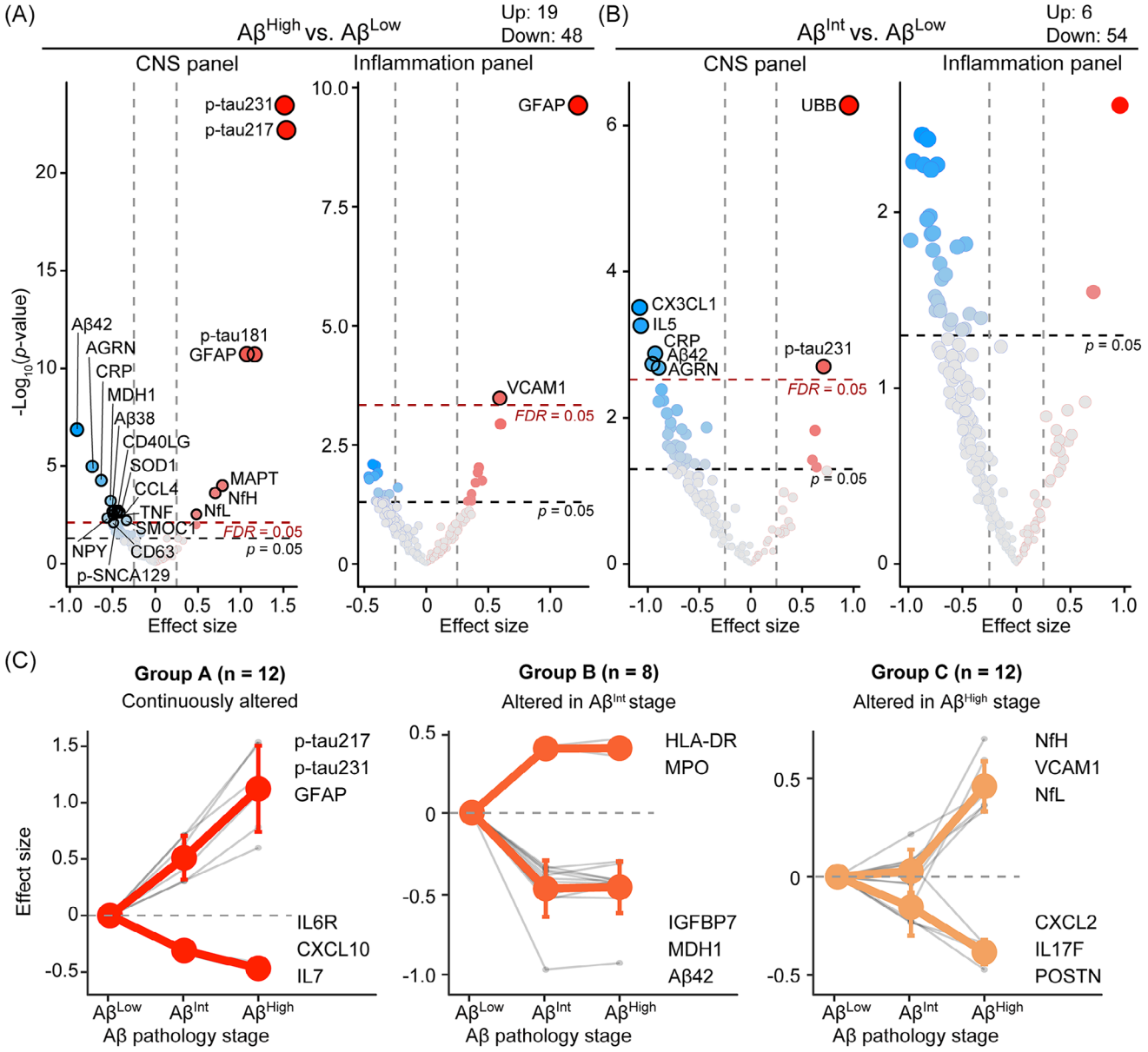

FIGURE 2 Plasma proteomic signatures at discrete stages of Aβ accumulation. A, B, Volcano plots showing the proteins dysregulated in the (A) $A\beta^{High}$ versus $A\beta^{Low}$ and (B) $A\beta^{Int}$ versus $A\beta^{Low}$ groups. Linear regression adjusted by age, sex, *APOE* ε4 genotype dose, and years of education. Blue and red dots represent down- and upregulated proteins, respectively, and dot size is proportional to *p* values (in−$\log_{10}$ scale). Gray and red dashed lines indicate the uncorrected *p* value threshold and the FDR-corrected threshold, respectively. Proteins with an FDR < 0.05 are highlighted in bold. C, Classification of protein groups defined by their dysregulation patterns across discrete Aβ pathology stages (Groups A–C). Within each protein group, the dots and error bars in color represent the mean value and standard deviation of the effect size on up- and downregulated proteins, with the gray dots and lines representing the effect size on each protein. Aβ, amyloid beta; *APOE*, apolipoprotein E; CNS, central nervous system; FDR, false discovery rate.

exhibited changes in the early stage of Aβ accumulation and showed continued dysregulation in the established stage (group A). Eight proteins (e.g., Aβ42 and HLA class II histocompatibility antigen, DR alpha chain) were dysregulated in the early stage and then stabilized (group B). Twelve proteins (e.g., neurofilament triplet protein, heavy subunit [NfH] and POSTN) were specifically dysregulated in the established stage of Aβ accumulation (group C), while 67 proteins (e.g., CCL24 and CX3CL1) were dysregulated only in the early stage (group D). Finally, 1 protein, chitinase-3-like protein 1 (CHI3L1), was downregulated in the early stage but upregulated in the established stage (group E). Notably, examination of the associations between these five blood protein groups and brain structural changes revealed distinct patterns (Figure S9 in supporting information). Group A and C proteins were most strongly associated with global brain region changes, corroborating their continuous roles in disease progression. In comparison, group B and D proteins were more strongly associated with brain regions that exhibit atrophy in the early stages of AD, including the hippocampus and middle temporal gyrus,[41] which is also consistent

with their dysregulation in the early stage of Aβ deposition. Hence, our blood proteome profiling by NULISAseq identified novel blood protein biomarkers associated with brain amyloid accumulation with distinct, stage-specific dysregulation patterns.

3.3 | Linear and non-linear proteomic dynamics along Aβ accumulation

Given the complex patterns of blood proteomic dysregulation in AD, to understand the dynamics of plasma protein alterations during Aβ accumulation, we examined the trajectories of blood protein level changes with increasing CL value and further performed hierarchical clustering analysis (Figure 3A). Most proteins (i.e., 268 proteins in clusters 2 and 3) exhibited a monotonic linear change across the AD continuum. Meanwhile, 57 proteins in clusters 1 and 4 followed U-shaped or inverted U-shaped trajectories with increasing Aβ accumulation, suggesting a non-linear association with Aβ pathology.

Therefore, to systematically identify blood proteins that exhibit a linear or non-linear dysregulation pattern, we performed linear regression analysis and generalized additive method analysis, respectively. As a result, we identified 27 proteins correlated with Aβ pathology in a linear manner ($p < 0.05$; Figure 3B and Table S7 in supporting information) and 23 proteins correlated with Aβ pathology in a non-linear manner (Edf > 2, $p < 0.05$; Figures 3C, S10; Table S8 in supporting information). Among them, 7 proteins exhibited both linear and non-linear characteristics.

To understand the biological meanings of these Aβ-associated plasma proteins, we performed co-regulation network analysis. The results yielded five different protein clusters with distinct co-regulation patterns and biological roles (Figure 3D). Protein cluster 1 contained ATN(I) biomarkers (i.e., p-tau217, p-tau231, p-tau181, microtubule associated protein tau [MAPT], and GFAP) and exhibited continuous upregulation throughout Aβ accumulation. Protein cluster 2, associated with synaptic transmission (e.g., CHI3L1, NfH, and acetylcholinesterase), and cluster 5, associated with leukocyte migration (e.g., fibroblast growth factor 21, CCL19, and C-reactive protein), also exhibited consistent up- and downregulation, respectively, plateauing at the late stage of Aβ pathology. In contrast, protein clusters 3 and 4 exhibited non-linear associations with Aβ pathology: at the initial stage of Aβ accumulation, proteins involved in the extracellular matrix (e.g., enolase 2 [ENO2], fms related receptor tyrosine kinase 3 ligand [FLT3LG], and ubiquitin C-terminal hydrolase L1 [UCHL1]) were downregulated while cytokine signaling proteins (e.g., CCL23, CCL14, and interleukin 18 binding protein) were upregulated; their regulation patterns reversed at the later stage of Aβ pathology. Together, these results reveal dynamic proteomic dysregulation during the progression of Aβ pathology, highlighting distinct dysregulation patterns and biological functions.

To investigate whether the plasma Aβ-associated proteins exhibit similar changes linked to Aβ pathology in the brain, we first examined whether these Aβ-associated proteins identified in plasma are also present as Aβ-associated proteins in the brains of AD patients.[28] Specifically, we examined the 27 plasma proteins that were linearly correlated with CL values for their association with Aβ plaque mean density in patients' brains. Seven proteins (i.e., AGRN, galectin 9 [LGALS9], SMOC1, CHI3L1, vascular cell adhesion molecule 1 (VCAM1), MAPT, and GFAP) were significantly associated with brain Aβ pathology (Table S9 in supporting information). Four of them (i.e., CHI3L1, VCAM1, MAPT, and GFAP) exhibited concordant changes between plasma and the brain, being positively correlated with Aβ plaque levels. In contrast, three proteins (i.e., AGRN, LGALS9, SMOC1) showed discordant changes between plasma and the brain, with their levels increasing in the brain but decreasing in plasma, being associated with Aβ plaque pathology (Figure S11 in supporting information). Furthermore, we examined the overlap between 23 plasma proteins non-linearly correlated with CL values and brain plaque mean density-associated proteins. Five proteins (i.e., CHI3L1, ENO2, GFAP, IL16, and UCHL1) were identified in both plasma and the brain (Table S9). Collectively, these findings suggest that specific plasma Aβ-associated proteins share brain proteomic signatures correlated with Aβ plaque pathology, highlighting potential molecular components of disease progression.

3.4 | Prediction of continuous Aβ accumulation using an eight-protein biomarker panel developed by machine learning

Given the identification of novel blood protein biomarkers associated with different stages of Aβ pathology, we investigated their potential for predicting continuous Aβ accumulation. Accordingly, we used a machine learning-based model, the LASSO model, to select protein candidates with the best predictive capabilities (Figure 4A). Through 100 iterations of randomly sampled data from 75% of the participants in our cohort, eight blood proteins, including p-tau217, p-tau231, POSTN, SMOC1, and KLK6 from the CNS 120 panel as well as CD4, NTF3, and PGF from the Inflammation 250 panel, were consistently selected by the model at least 75 times (Figure 4B). Among these eight proteins, p-tau217, p-tau231, NTF3, and PGF were positively associated with Aβ pathology, while CD4, POSTN, SMOC1, and KLK6 were negatively associated (Figure 4C). Specifically, p-tau217 and p-tau231 levels increased consistently across the AD continuum, while NTF3 and PGF levels were primarily elevated in the later stages (Figure 4D). In contrast, POSTN and KLK6 levels declined as Aβ accumulated, while CD4 and SMOC1 levels showed more complex trajectories, being upregulated in the early stage of disease progression but downregulated in the later stage (Figure 4D).

Next, we evaluated the performance of machine learning-based models that included the eight abovementioned blood proteins together with age and sex as covariates for predicting Aβ pathology. We tested five types of machine learning models: RF, XGB, SVM, LASSO, and the GLM. The SVM-derived model showed the highest predictive accuracy and robustness in both the training dataset ($r = 0.86$, $p < 2.2 \times 10^{-16}$, root mean square error [RMSE] = 19.89) and testing dataset ($r = 0.89$, $p < 2.2 \times 10^{-16}$, RMSE = 12.69; Figure 4E and Table S10 in supporting information). Compared to the SVM-derived

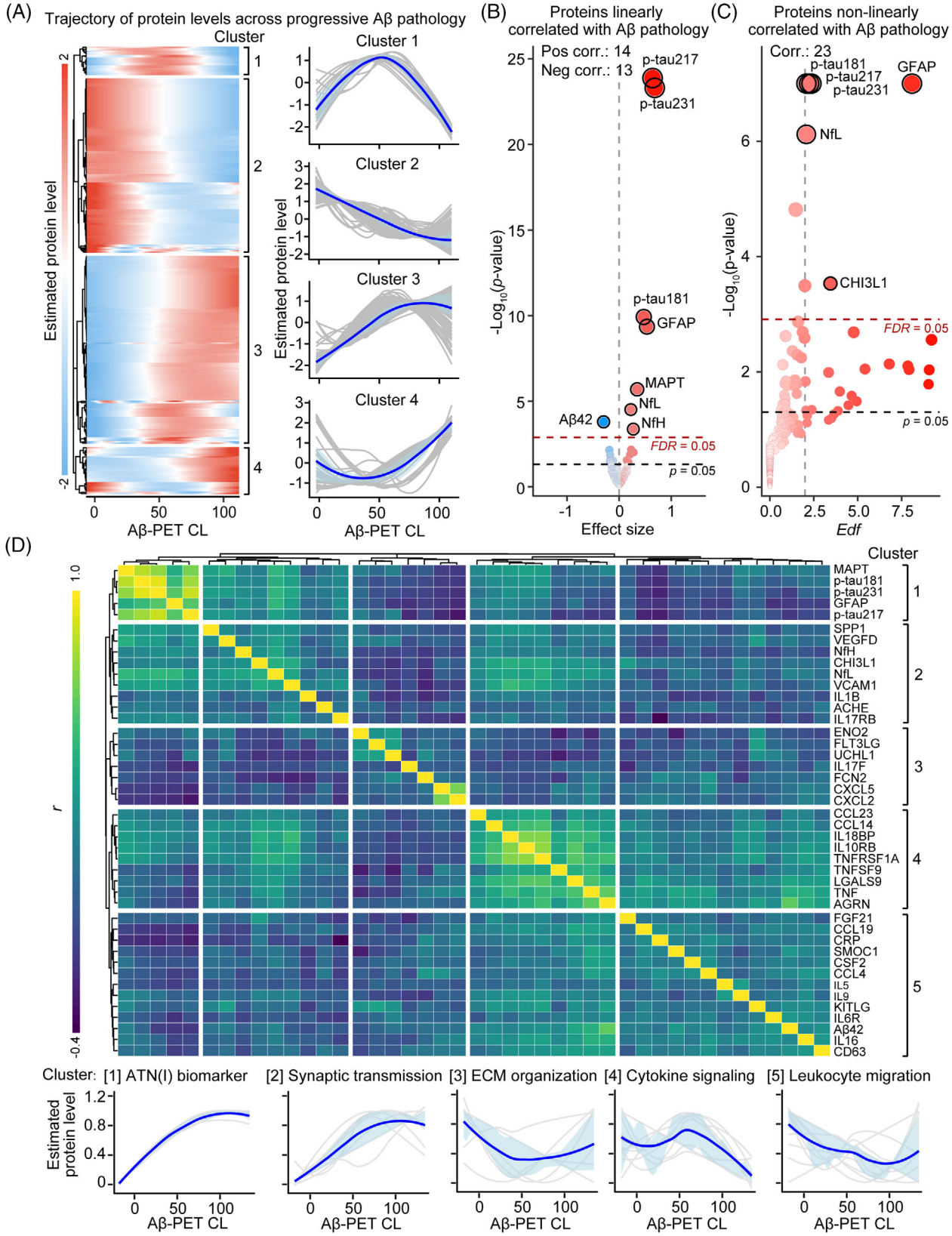

FIGURE 3 Plasma protein trajectories along continuous progression of Aβ pathology. A, Trajectory of protein alterations alongside Aβ accumulation. Left panel: Heatmap showing estimated protein level trajectories along increasing Aβ PET CL values, adjusted by age, sex, *APOE* ε4 genotype dose, and years of education. Each line represents a distinct protein. Colors indicate the estimated protein level, with blue and red representing below- and above-average levels, respectively. Right panel: LOESS plots show protein trajectories within each cluster. B, C, Volcano

model, the RF- and XGB-derived models achieved higher accuracy in the training dataset (r_{RF} = 0.96, r_{XGB} = 0.97, both $p < 2.2 \times 10^{-16}$) but lower accuracy in the testing dataset (r_{RF} = 0.81, r_{XGB} = 0.81, both $p < 2.2 \times 10^{-16}$), suggesting a high risk of overfitting. Therefore, we selected the SVM-derived model ("CL predictor" hereafter) for further analysis. For predicting Aβ pathology, the CL predictor significantly outperformed each individual protein, including p-tau217 (r = 0.77, $p < 2.2 \times 10^{-16}$), p-tau231 (r = 0.65, $p < 2.2 \times 10^{-16}$), and CD3 (r = 0.43, $p < 0.05$; Figure 4F and Table S11 in supporting information). To further investigate the predictive contribution of each protein in the CL predictor, we performed SHAP value analysis. Overall, p-tau217 (mean[|SHAP value|] = 16.18) and p-tau231 (mean[|SHAP value|] = 14.08) contributed most to the prediction outcome of the CL predictor. The remaining six proteins exhibited smaller influences (mean[|SHAP value|]: CD4 = 3.51, KLK6 = 3.38, SMOC1 = 3.09, POSTN = 3.04, NTF3 = 2.73, and PGF = 2.14; Figure S12 in supporting information). We further conducted a detailed per-sample analysis of feature contributions and interactions, revealing that these six proteins had high SHAP values in the prediction of certain samples and contributed to improved prediction precision. These findings suggest that although these proteins have limited overall importance across the dataset, they play a critical role in accurately predicting individual cases (Figures 4G, S13 in supporting information).

3.5 | Classification of early Aβ pathology by the eight-protein CL predictor

As mentioned above, existing blood ATN biomarkers lack sufficient accuracy for classifying the early stage of Aβ pathology (maximum AUC = 0.81 for $A\beta^{Int}$ vs. $A\beta^{Low}$; Figure 1F). Given that the eight-protein CL predictor predicted continuous Aβ accumulation better than the traditional blood ATN biomarkers, we investigated whether this panel also enhances the detection and staging of Aβ pathology. While both the eight-protein CL predictor and p-tau217 showed high accuracy for detecting established Aβ pathology ($AUC_{CL\ predictor}$ = 0.99 and $AUC_{p\text{-}tau217}$ = 0.97 for $A\beta^{High}$ vs. $A\beta^{Low}$; Figure S14 in supporting information), the eight-protein CL predictor classified the early stage of Aβ pathology more accurately than p-tau217 or p-tau231 ($AUC_{CL\ predictor}$ = 0.93, $AUC_{p\text{-}tau217}$ = 0.78, and $AUC_{p\text{-}tau231}$ = 0.79 for $A\beta^{Int}$ vs. $A\beta^{Low}$; Figure 4H). The eight-protein CL predictor also showed higher sensitivity and specificity ($sensitivity_{CL\ predictor}$ = 0.99, $sensitivity_{p\text{-}tau217}$ = 0.78, $sensitivity_{p\text{-}tau231}$ = 0.91, $specificity_{CL\ predictor}$ = 0.84, $specificity_{p\text{-}tau217}$ = 0.76, $specificity_{p\text{-}tau217}$ = 0.67 for $A\beta^{Int}$ vs. $A\beta^{Low}$). Furthermore, the eight-protein CL predictor outperformed p-tau217 in differentiating the early and established stages of Aβ pathology ($AUC_{CL\ predictor}$ = 0.89, $AUC_{p\text{-}tau217}$ = 0.83, and $AUC_{p\text{-}tau231}$ = 0.82 for $A\beta^{Int}$ vs. $A\beta^{High}$; Figure 4I), suggesting that the panel is better suited for staging Aβ pathology. In addition, to validate the specificity of the eight-protein CL predictor and p-tau217 for detecting Aβ pathology, we assessed their performance in a small cohort of 12 patients with $A\beta^{+}$AD and 12 with $A\beta^{-}$non-AD dementia. Consistently, both the eight-protein CL predictor and p-tau217 showed comparably high performance in differentiating patients with $A\beta^{+}$ from those with $A\beta^{-}$ non-AD dementia ($AUC_{CL\ predictor}$ = 0.996 and $AUC_{p\text{-}tau217}$ = 0.987 for $A\beta^{+}$ AD vs. $A\beta^{-}$ non-AD dementia; Figure 4J). Thus, our results demonstrate that the eight-protein CL predictor not only accurately predicts continuous Aβ accumulation, but is also more accurate for detecting early Aβ pathology than traditional blood ATN biomarkers.

4 | DISCUSSION

Given the emergence of blood-based biomarkers as promising tools for diagnosing and managing AD, it is crucial to develop assays to accurately quantify Aβ pathology. In this study, we comprehensively profiled the plasma proteome of individuals with varying degrees of Aβ pathology and identified 43 proteins significantly linearly or non-linearly correlated with Aβ levels. Notably, these Aβ-associated proteins exhibit unique dysregulation patterns as Aβ pathology progresses and are involved in distinct biological processes, such as innate immunity, adaptive immunity, and angiogenesis. These findings suggest that the plasma proteome undergoes dynamic alterations throughout Aβ accumulation, indicating that evaluating proteins with distinct trajectories is a potential strategy for accurately quantifying Aβ levels. Based on these insights, we used machine learning methods to select a panel of eight proteins with unique dysregulation patterns. We constructed a model termed the CL predictor, which predicts CL values more accurately than plasma p-tau217 or p-tau231 (r = 0.89 vs.

plots illustrating the (B) linear and (C) non-linear correlations between protein levels and CL values. B, Volcano plot illustrating the linear correlation between protein level and CL values. The analysis was adjusted by age, sex, *APOE* ε4 genotype dose, and years of education. Blue and red dots represent down- and upregulated proteins, respectively. C, Volcano plot showing the non-linear correlations between protein levels and CL values. Dot color intensity is proportional to Edf. D, Biological processes related to the Aβ pathology-associated proteins. Upper panel: Heatmap displaying pairwise correlations among plasma proteins correlated with Aβ accumulation. Each row and column represents one protein, with color intensity indicating the strength and direction of correlation. Lower panel: LOESS plots show the representative trajectories within each cluster. In volcano plots, dot size is proportional to the p value (in $-\log_{10}$ scale), the gray dashed line indicates the uncorrected p value threshold, and the red dashed line indicates the FDR-corrected threshold. Proteins with an FDR < 0.05 are shown in bold text. In the LOESS plots, each gray line represents a distinct protein, and the blue line represents the representative trajectories defined by the median value within each cluster, with the 0.25 and 0.75 quantile intervals shown in light blue. Aβ, amyloid beta; *APOE*, apolipoprotein E; CL, Centiloid; CNS, central nervous system; ECM, extracellular matrix; Edf, effective degrees of freedom; FDR, false discovery rate; LOESS, locally estimated scatterplot smoothing; PET, positron emission tomography.

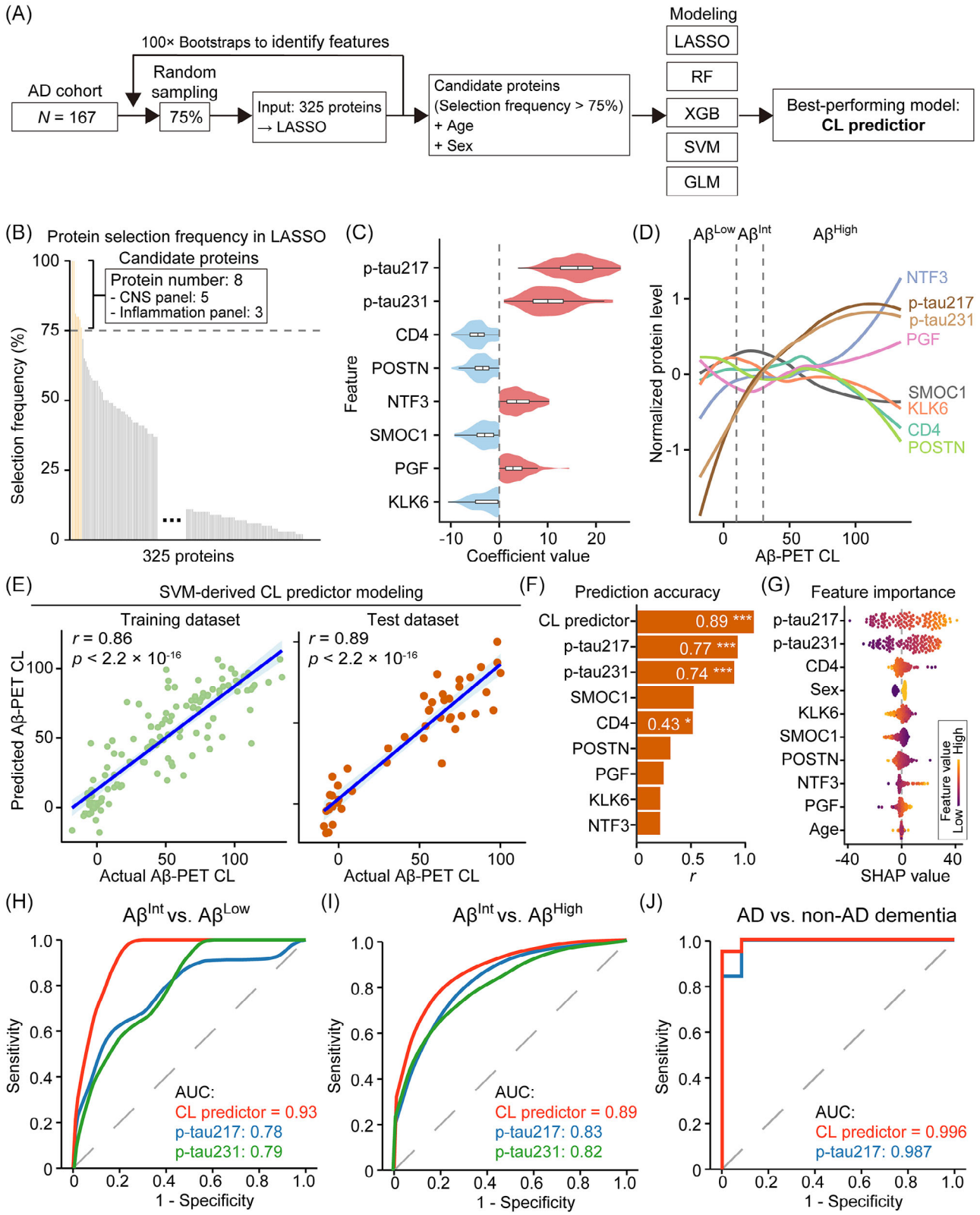

FIGURE 4 Machine learning-based modeling of a plasma protein panel for predicting Aβ pathology on a continuous scale. A, Study workflow. B, Bar plot depicting the selection frequency for identifying the most informative proteins across iterations by bootstrapping and the LASSO regression model. Proteins consistently selected in > 75% of bootstrap samples (i.e., eight proteins) constitute the Aβ pathology prediction panel (termed the "CL predictor"). C, Violin plot showing the distribution of bootstrap-derived coefficients for candidate proteins, reflecting their relative importance in model selection. D, LOESS plot showing the trajectories of proteins in the CL predictor against Aβ PET CL values. The first and second dashed lines correspond to early Aβ pathology (CL = 10) and established Aβ pathology (CL = 30), respectively. E, Correlations between actual Aβ PET CL values and predicted values by the CL predictor were evaluated separately in the training dataset ($r = 0.86$, $p < 2.2\times 10^{-16}$) and

$r_{p\text{-}tau217}$ = 0.77, $r_{p\text{-}tau231}$ = 0.74, respectively). Furthermore, the CL predictor is more sensitive in identifying individuals with early Aβ accumulation (AUC = 0.93 vs. $AUC_{p\text{-}tau217}$ = 0.78, $AUC_{p\text{-}tau231}$ = 0.79, respectively), facilitating the identification of high-risk populations. Collectively, these findings highlight the potential of blood-based biomarkers for the early detection, precise staging, and efficacy monitoring of Aβ pathology, offering a promising tool for clinical practice and trials of Aβ-targeting therapeutic strategies.

Quantifying Aβ PET using the CL scale is a robust and widely used approach for quantifying Aβ pathology.[4,5] The CL scale supports identification of individuals eligible for anti-Aβ therapy, monitoring of reductions in Aβ deposition after treatment, and decisions on therapeutic endpoints.[42] Identifying plasma protein biomarkers associated with CL values could be a more cost effective and accessible alternative to Aβ PET. In this study, we show that the plasma proteome exhibits stage-dependent alterations during Aβ accumulation (Figures 2C, S5; Table S6). Alongside well-known biomarkers (e.g., p-tau217), adaptive immunity-related proteins, including IL-17B (interleukin-17B)[43] and IL-7 (interleukin-7),[44] are monotonically associated with brain Aβ accumulation. This is consistent with findings that stronger adaptive immune responses are correlated with greater AD severity.[45] Importantly, we found some proteins that exhibit stage-specific dysregulation. For example, among individuals with established Aβ pathology, proteins linked to neuronal integrity (e.g., NfL[46]) and vascular function (e.g., VCAM1[47]) are specifically dysregulated, which is consistent with evidence that axonal degeneration and cerebrovascular dysfunction become more prominent in the later stages of AD. Interestingly, innate immunity-related proteins, such as TNFSF14 (TNF superfamily member 14)[40] and CX3CL1 (C-X3-C motif chemokine ligand 1),[48] are specifically dysregulated in the early stage. Previous investigations of the plasma levels of these innate immune mediators in AD and healthy individuals have yielded conflicting results as to whether and to what extent dysregulation occurs.[49–51] Our results may suggest that their levels follow a non-linear trajectory across AD progression, exhibiting early dysregulation followed by reversal. Concordant with previous studies,[52,53] these stage-dependent alterations support that systemic proteomic changes—not limited to pathological biomarkers—are strongly associated with the advancement of Aβ pathology. Interestingly, our analysis reveals several proteins associated with Aβ plaques in both plasma and the brain. Among them, proteins related to inflammatory response (e.g., CHI3L1) showed concordant relationships between plasma and the brain, whereas those related to nervous system development (e.g., AGRN) exhibited discordant relationships. These results suggest that the relationship between plasma and brain protein levels may vary during the progression of Aβ pathology depending on specific pathways. Understanding these compartment-specific protein dynamics may help uncover the biology of Aβ pathology.

While blood biomarkers are promising diagnostic tools for Aβ pathology,[54] they are not yet clinically implemented for biological staging. By itself, the leading candidate, p-tau217, is not effective for staging given its insufficient AUC in differentiating $A\beta^{Int}$ and $A\beta^{High}$ individuals. This may be because the plasma levels of these biomarkers change significantly during early pathogenesis but then level off as Aβ continues to accumulate.[10,55–57] Thus, although these biomarkers can indicate positivity or negativity of Aβ pathology, they are not reflective of the cumulative amount of Aβ. In the latest AD framework,[13] the National Institute on Aging–Alzheimer's Association (NIA-AA) Working Group outlines a conceptual fluid-only staging scheme that is based on the sequence of abnormal biomarker emergence, starting with p-tau (i.e., p-tau181, p-tau217, or p-tau231), followed by p-tau205, then MTBR-tau243, and finally non-phosphorylated mid-domain tau fragments. This highlights the potential of combining biomarkers with distinct temporal dynamics for staging. Accordingly, we harnessed advanced machine learning techniques to capture interaction patterns and non-linear relationships among blood proteins. This yielded an eight-protein panel, termed the CL predictor, comprising p-tau217, p-tau231, CD4, NTF3, PGF, SMOC1, KLK6, and POSTN. Each of these proteins has been reported to be associated with AD through distinct pathological pathways: p-tau217 and p-tau231 indicate pathological progression; CD4 denotes immune-cell regulation[58]; NTF3 promotes neuronal survival[59]; PGF drives angiogenesis[60]; and SMOC1,[12] KLK6,[61] and POSTN[62] coordinate extracellular matrix remodeling and leukocyte migration.

By integrating these blood proteins, the CL predictor improves the precision of blood-based Aβ pathology quantification. Its output is more strongly correlated with CL values than its individual constituent biomarker proteins. Notably, the CL predictor better detects intermediate-range Aβ pathology (i.e., CL 10–30) than individual biomarkers. This range, linked to an elevated risk of cognitive decline,

test dataset ($r = 0.89$, $p < 2.2\times 10^{-16}$). The linear regression line with 95% confidence intervals, Spearman correlation coefficients (r), and p values are shown. F, Bar plot comparing the prediction accuracy of the CL predictor and its individual protein components. Spearman correlation coefficients (r) and p values are only shown for proteins exhibiting a significant correlation (i.e., $p < 0.05$). G, Beeswarm plot showing the SHAP value of each feature in each sample. Color indicates the value of the feature. H–J, ROC curves comparing the classification performance of the CL predictor and p-tau217 for distinguishing (H) individuals in the $A\beta^{Int}$ group from those in the $A\beta^{Low}$ group as well as (I) individuals in the $A\beta^{Int}$ group from those in the $A\beta^{High}$ group. H, Classification of the $A\beta^{Int}$ versus $A\beta^{Low}$ groups (CL predictor AUC = 0.93, p-tau217 AUC = 0.78, p-tau231 AUC = 0.79). I, Classification of the $A\beta^{Int}$ versus $A\beta^{High}$ groups (CL predictor AUC = 0.89, p-tau217 AUC = 0.83, p-tau231 AUC = 0.82). J, ROC curves comparing the classification performance of the CL predictor and p-tau217 for distinguishing individuals with clinically diagnosed AD or non-AD dementia (CL predictor AUC = 0.996, p-tau217 AUC = 0.987). *$p < 0.05$, ***$p < 0.001$. Aβ, amyloid beta; AD, Alzheimer's disease; AUC, area under the receiver operating characteristic curve; CL, Centiloid; CNS, central nervous system; GLM, generalized linear model; LASSO, least absolute shrinkage and selection operator; LOESS, locally estimated scatterplot smoothing; PET, positron emission tomography; p-tau, phosphorylated tau; RF, random forest; ROC, receiver operating characteristic; SHAP, SHapley Additive exPlanations; SVM, support vector machine; XGB, XGBoost.

is a critical inflection point in AD progression and represents a window for therapeutic intervention.[42] With high accuracy and accessibility, the CL predictor could broaden the use of blood-based biomarkers in clinical practice, supporting both early diagnosis and effective patient management. Specifically, it can expand the scale of screening to enrich clinical cohorts, particularly for early prevention studies such as the AHEAD study.[63] For patients, the CL predictor would facilitate an increased frequency of testing to track Aβ accumulation, assess progression risk, and guide eligibility for anti-Aβ therapies. Moreover, the CL predictor could serve as a pharmacodynamic indicator that precisely indicates the change in Aβ pathology after treatment to inform clinical decisions. Hence, the CL predictor provides a practical blood-based quantitative assessment of Aβ pathology and has the potential to enhance early diagnosis, clinical management, and therapeutic development for AD.

Advances in quantitative protein profiling have generated abundant molecular fluid datasets, and machine learning is increasingly important for translating these datasets into clinical applications, especially in biomarker discovery.[20] Machine learning has been applied to identify candidate biomarkers for AD,[64] Parkinson's disease,[65] and Huntington's disease.[66] In our analysis, LASSO regression with repeated random resampling and cross-validation reduced 325 protein candidates to a small and highly informative feature set. Bootstrapping, only retaining features present in > 75% of runs, enhanced the stability and reproducibility of predictors identified by LASSO regression. Cross-validation[67] further provided unbiased performance estimates, mitigating overfitting. Together, these complementary strategies enhanced the robustness of feature selection. After these steps, we divided the data into training (75%) and test (25%) datasets to construct and compare five models: LASSO regression, GLM, RF, SVM, and XGB. The SVM model outperformed the others in predicting CL values and showed comparable performance in the training and test datasets, demonstrating good generalization. This may be attributable to its capacity to manage high-dimensional data and model complex, non-linear relationships via kernel functions while maintaining strong generalization through margin-based regularization.[20,68] This balanced strategy appears to be suitable for the sample size and feature space of our dataset. In contrast, the predictive accuracy of the ensemble tree methods, RF and XGB, was markedly lower on the test dataset than on the training dataset. This may suggest that these models overfit the training data,[69] therefore resulting in diminished performance when applied to unseen data. In addition, the LASSO regression and GLM models performed consistently but less accurately than the SVM model, likely because of their limited capacity to capture non-linear relationships.[70] Taken together, considering its high predictive accuracy and generalization, we demonstrate that the SVM model is feasible for integrating multiple protein biomarkers to accurately indicate disease status.

Further validation and optimization will promote the clinical translation of the CL predictor. While our analysis demonstrates associations between protein levels and Aβ accumulation, further longitudinal study will help validate the temporal evolution of these proteins. In addition, the robustness of the CL predictor, particularly for individuals in the intermediate range of Aβ accumulation, may be constrained by the limited sample size. Therefore, validation in larger cohorts is essential to enable the clinical translation of our model. Furthermore, in addition to Aβ pathology, recently published AD staging criteria highlight the importance of assessing the location and extent of brain tau accumulation (i.e., $A\beta^+$ tau_2^-, $A\beta^+$ tau_{2MTL}^+, $A\beta^+$ tau_{2MOD}^+, and $A\beta^+$ tau_{2HIGH}^+).[13] Future investigations of blood biomarkers for both Aβ and tau pathology will provide insights for more comprehensive blood-based staging of AD.

In summary, we comprehensively profiled the plasma proteome dynamics during Aβ accumulation, identified novel proteins associated with Aβ accumulation, and developed a high-performance, eight-protein panel for accurately quantifying Aβ pathology. Our findings demonstrate the feasibility of integrating multiple plasma proteins to improve the linear correlation between blood-based biomarkers and cerebral Aβ pathology, thereby facilitating the early diagnosis, staging, and prognosis of AD. Furthermore, our study provides crucial insights for patient selection and management in clinical practice and trials, particularly for emerging Aβ-targeting therapies, thereby paving the way for advanced AD diagnostics and therapeutics.

AUTHOR CONTRIBUTIONS

W.Z., Y.J., A.K.Y.F., and N.Y.I. conceived of the study; H.Y.W., E.Y.L.C., B.W.Y.W., R.M.N.L., S.K.L., F.C.I., W.M.W., C.K.S., H.M.W., J.K.Y.Y., Y.F.S., V.C.T.M., and T.C.Y.K. organized patient recruitment and sample collection; W.Z., Y.J., L.K.W.C., and E.Y.L.C. performed the experiments; W.Z. and Y.J. set up the data-processing pipelines; W.Z., Y.J., W.W.W., H.Y.W., L.K.W.C., F.C.I., K.Y.M., A.H., J.H., H.Z., A.K.Y.F., and N.Y.I. analyzed the data; and W.Z., Y.J., A.K.Y.F., and N.Y.I. wrote the manuscript with input from all authors.

ACKNOWLEDGMENTS

The authors would like to express their sincerest gratitude to the participants from the Hong Kong Chinese cohort, along with their relatives, at the Prince of Wales Hospital of the Chinese University of Hong Kong (CUHK-PWH), Queen Mary Hospital (QMH), United Christian Hospital (UCH), and Tuen Mun Hospital (TMH), without whom this research would have not been possible. The authors also thank Patrick Ka Chun Chiu (QMH), Dr. Ka Keung Yam (QMH), Dr. Edmond Kwok Yiu Sha (UCH), Dr. Ting Kwan Yim (UCH), Dr. Sze Yuen Fung (UCH), Dr. Ping Cheong Ho (UCH), Dr. Kathy Ka Ling Wong (UCH), Dr. Iki Hoi Ki Chan (UCH), Yuen Yee Tam (UCH), Mei Ling Lau (UCH), Ka Shing Ho (TMH), Tung Yi Fu (TMH), Hiu Ki Yam (TMH), and Chung Ho Chan (TMH) for coordinating the collection of clinical samples and data. Y.J. is a recipient of the Hong Kong Postdoctoral Fellowship Award from the Research Grants Council of the Hong Kong Special Administrative Region, China (Project No. HKUST PDFS2324-6S04). H.Z. is a Wallenberg Scholar and a Distinguished Professor at the Swedish Research Council supported by grants from the Swedish Research Council (#2023-00356, #2022-01018, and #2019-02397), the European Union's Horizon Europe Research and Innovation Programme

under grant agreement No. 101053962, Swedish State Support for Clinical Research (#ALFGBG-71320), the Alzheimer Drug Discovery Foundation (ADDF), USA (#201809-2016862), the AD Strategic Fund and the Alzheimer's Association (#ADSF-21-831376-C, #ADSF-21-831381-C, #ADSF-21-831377-C, and #ADSF-24-1284328-C), the European Partnership on Metrology co-financed by the European Union's Horizon Europe Research and Innovation Programme and the Participating States (NEuroBioStand, #22HLT07), the Bluefield Project, Cure Alzheimer's Fund, the Olav Thon Foundation, the Erling-Persson Family Foundation, Familjen Rönströms Stiftelse, Familjen Beiglers Stiftelse, Stiftelsen för Gamla Tjänarinnor, Hjärnfonden, Sweden (#FO2022-0270), the European Union's Horizon 2020 Research and Innovation Programme under the Marie Skłodowska-Curie grant agreement No. 860197 (MIRIADE), the European Union Joint Programme – Neurodegenerative Disease Research (JPND2021-00694), the National Institute for Health and Care Research University College London Hospitals Biomedical Research Centre, the UK Dementia Research Institute at UCL (UKDRI-1003), and an anonymous donor.

This study was supported in part by the Research Grants Council of Hong Kong (the Collaborative Research Fund [C6027-19GF], the Theme-Based Research Scheme [T13-605/18 W], and the General Research Fund [HKUST16103122, HKUST16104624, and HKUST16102824]), the Areas of Excellence Scheme of the University Grants Committee (AoE/M-604/16), the InnoHK initiative of the Innovation and Technology Commission of the Hong Kong Special Administrative Region Government (ITCPD/17-9), the SIAT–HKUST Joint Laboratory for Brain Science (Joint Laboratory Funding Scheme [JLFS/M-604/24]), and the Guangdong–Hong Kong Joint Laboratory for Psychiatric Disorders (2023B1212120004).

CONFLICT OF INTEREST STATEMENT

Y.J., F.C.I., A.K.Y.F., and N.Y.I. are inventors of related technology licensed to Cognitact. Y.J. and F.C.I. are co-founders of Cognitact. J.H. has served as a consultant for Eli Lilly and Eisai. H.Z. has served on scientific advisory boards and/or as a consultant for Abbvie, Acumen, Alector, Alzinova, ALZpath, Amylyx, Annexon, Apellis, Artery Therapeutics, AZTherapies, Cognito Therapeutics, CogRx, Denali, Eisai, Enigma, LabCorp, Merck Sharp & Dohme, Merry Life, Nervgen, Novo Nordisk, Optoceutics, Passage Bio, Pinteon Therapeutics, Prothena, Quanterix, Red Abbey Labs, reMYND, Roche, Samumed, ScandiBio Therapeutics AB, Siemens Healthineers, Triplet Therapeutics, and Wave; has given lectures sponsored by Alzecure, BioArctic, Biogen, Cellectricon, Fujirebio, LabCorp, Lilly, Novo Nordisk, Oy Medix Biochemica AB, Roche, and WebMD; is a co-founder of Brain Biomarker Solutions in Gothenburg AB (BBS), which is a part of the GU Ventures Incubator Program; and is a shareholder of MicThera (outside submitted work). All other authors declare no conflicts of interest. Author disclosures are available in the supporting information.

DATA AVAILABILITY STATEMENT

All statistical data associated with this study are contained in the main text or supporting information. The consent forms signed by participants from the Hong Kong Chinese cohort state that the research content will be kept private under the supervision of the hospital and research team. Therefore, the phenotypic and proteomic data of individual participants will only be available and shared in the context of a formal collaboration. A review panel hosted at the Hong Kong University of Science and Technology will process and review any applications for data sharing and project collaboration, and promptly notify applicants of their decision. Researchers may contact sklneurosci@ust.hk for details about data sharing and project collaboration related to the present study.

ORCID

Nancy Y. Ip https://orcid.org/0000-0002-2763-8907

REFERENCES

1. Duyckaerts C, Delatour B, Potier M-C. Classification and basic pathology of Alzheimer disease. *Acta Neuropathol*. 2009;118(1):5-36. doi:10.1007/s00401-009-0532-1
2. McKhann GM, Knopman DS, Chertkow H, et al. The diagnosis of dementia due to Alzheimer's disease: Recommendations from the National Institute on Aging-Alzheimer's Association workgroups on diagnostic guidelines for Alzheimer's disease. *Alzheimer's Dement*. 2011;7(3):263-269. doi:10.1016/j.jalz.2011.03.005
3. Ikonomovic MD, Buckley CJ, Heurling K, et al. Post-mortem histopathology underlying β-amyloid PET imaging following flutemetamol F 18 injection. *Acta Neuropathol Commun*. 2016;4(1):130. doi:10.1186/s40478-016-0399-z
4. Collij LE, Bollack A, La Joie R, et al. Centiloid recommendations for clinical context-of-use from the AMYPAD consortium. *Alzheimer's Dement*. 2024;20(12):9037-9048. doi:10.1002/alz.14336
5. Iaccarino L, Burnham SC, Tunali I, et al. A practical overview of the use of amyloid-PET Centiloid values in clinical trials and research. *NeuroImage: Clin*. 2025;46:103765. doi:10.1016/j.nicl.2025.103765
6. Cummings JL. Maximizing the benefit and managing the risk of anti-amyloid monoclonal antibody therapy for Alzheimer's disease: Strategies and research directions. *Neurotherapeutics*. 2025;22(3):e00570. doi:10.1016/j.neurot.2025.e00570
7. Nakamura A, Kaneko N, Villemagne VL, et al. High performance plasma amyloid-β biomarkers for Alzheimer's disease. *Nature*. 2018;554(7691):249-254. doi:10.1038/nature25456
8. Jack Jr CR, Bennett DA, Blennow K, et al. NIA-AA Research Framework: Toward a biological definition of Alzheimer's disease. *Alzheimer's Dement*. 2018;14(4):535-562. doi:10.1016/j.jalz.2018.02.018
9. Palmqvist S, Warmenhoven N, Anastasi F, et al. Plasma phospho-tau217 for Alzheimer's disease diagnosis in primary and secondary care using a fully automated platform. *Nat Med*. 2025;31(6):2036-2043. doi:10.1038/s41591-025-03622-w
10. Milà-Alomà M, Ashton NJ, Shekari M, et al. Plasma p-tau231 and p-tau217 as state markers of amyloid-β pathology in preclinical Alzheimer's disease. *Nat Med*. 2022;28(9):1797-1801. doi:10.1038/s41591-022-01925-w
11. Montoliu-Gaya L, Benedet AL, Tissot C, et al. Mass spectrometric simultaneous quantification of tau species in plasma shows differential associations with amyloid and tau pathologies. *Nat Aging*. 2023;3(6):661-669. doi:10.1038/s43587-023-00405-1
12. Pichet Binette A, Gaiteri C, Wennström M, et al. Proteomic changes in Alzheimer's disease associated with progressive Aβ plaque and tau tangle pathologies. *Nat Neurosci*. 2024;27(10):1880-1891. doi:10.1038/s41593-024-01737-w
13. Jack Jr CR, Andrews JS, Beach TG, et al. Revised criteria for diagnosis and staging of Alzheimer's disease: Alzheimer's Association Workgroup. *Alzheimer's Dement*. 2024;20(8):5143-5169. doi:10.1002/alz.13859

14. Bucci M, Bluma M, Savitcheva I, et al. Profiling of plasma biomarkers in the context of memory assessment in a tertiary memory clinic. *Transl Psychiatry*. 2023;13(1):268. doi:10.1038/s41398-023-02558-4
15. Rissman RA, Langford O, Raman R, et al.; Team, for the A. 3-45 S. Plasma Aβ42/Aβ40 and phospho-tau217 concentration ratios increase the accuracy of amyloid PET classification in preclinical Alzheimer's disease. *Alzheimer's Dement*. 2024;20(2):1214-1224. doi:10.1002/alz.13542
16. Feng W, Beer JC, Hao Q, et al. NULISA: A proteomic liquid biopsy platform with attomolar sensitivity and high multiplexing. *Nat Commun*. 2023;14(1):7238. doi:10.1038/s41467-023-42834-x
17. Di Molfetta G, Pola I, Tan K, et al. Inflammation biomarkers and Alzheimer's disease: A pilot study using NULISAseq. *Alzheimer's Dement: Diagn Assess Dis Monit*. 2025;17(1):e70079. doi:10.1002/dad2.70079
18. Rea Reyes RE, Wilson RE, Langhough RE, et al. Targeted proteomic biomarker profiling using NULISA in a cohort enriched with risk for Alzheimer's disease and related dementias. *Alzheimer's Dement*. 2025;21(5):e70166. doi:10.1002/alz.70166
19. Zeng X, Sehrawat A, Lafferty TK, et al. Novel plasma biomarkers of amyloid plaque pathology and cortical thickness: Evaluation of the NULISA targeted proteomic platform in an ethnically diverse cohort. *Alzheimer's Dement*. 2025;21(2):e14535. doi:10.1002/alz.14535
20. Swanson K, Wu E, Zhang A, Alizadeh AA, Zou J. From patterns to patients: Advances in clinical machine learning for cancer diagnosis, prognosis, and treatment. *Cell*. 2023;186(8):1772-1791. doi:10.1016/j.cell.2023.01.035
21. Nasreddine ZS, Phillips NA, Bédirian V, et al. The montreal cognitive assessment, MoCA: A brief screening tool for mild cognitive impairment. *J Am Geriatr Soc*. 2005;53(4):695-699. doi:10.1111/j.1532-5415.2005.53221.x
22. Pangman VC, Sloan J, Guse L. An examination of psychometric properties of the mini-mental state examination and the standardized mini-mental state examination: Implications for clinical practice. *Appl Nurs Res*. 2000;13(4):209-213. doi:10.1053/apnr.2000.9231
23. Robin X, Turck N, Hainard A, et al. pROC: An open-source package for R and S+ to analyze and compare ROC curves. *BMC Bioinf*. 2011;12, p.77. doi:10.1186/1471-2105-12-77
24. Davis J, Goadrich M. The relationship between precision-recall and ROC curves. *Proceedings of the 23rd International Conference on Machine Learning*, 2006;233-240. doi:10.1145/1143844.1143874
25. Maechler M, Rousseeuw P, Croux C, et al. robustbase: Basic Robust Statistics R package version 0.99-6. 2025. https://cran.r-project.org/web/packages/robustbase/index.html
26. Wood SN. Fast Stable Restricted Maximum Likelihood and Marginal Likelihood Estimation of Semiparametric Generalized Linear Models. *J R Stat Soc B: Stat Methodol*. 2011;73(1):3-36. doi:10.1111/j.1467-9868.2010.00749.x
27. R Core Team. R: A Language and Environment for Statistical Computing. R Foundation for Statistical Computing; 2023. https://www.r-project.org/
28. Wang E, Yu K, Cao J, et al. Multiscale proteomic modeling reveals protein networks driving Alzheimer's disease pathogenesis. *Cell*. 2025;188(22):6186-6204. doi:10.1016/j.cell.2025.08.038
29. Friedman J, Hastie T, Tibshirani R. Regularization paths for generalized linear models via coordinate descent. *J Stat Softw*. 2010;33(1):1-22.
30. Liaw A, Wiener M. Classification and Regression by randomForest. *R News*. (n.d.);2(3):18-22. https://CRAN.R-project.org/doc/Rnews/
31. Chen T, He T, Benesty M, et al. xgboost: Extreme Gradient Boosting. 2025. doi:10.32614/CRAN.package.xgboost
32. Meyer D, Dimitriadou E, Hornik K, et al. e1071: Misc Functions of the Department of Statistics, Probability Theory Group (Formerly: E1071), TU Wien. 2024. doi:10.32614/CRAN.package.e1071
33. Mayer M, Watson D, Biecek P. kernelshap: Kernel SHAP (0.9.0). 2025 https://cran.r-project.org/web/packages/kernelshap/index.html
34. Mayer M, Stando A. shapviz: SHAP visualizations (0.10.2). 2025 https://cran.r-project.org/web/packages/shapviz/index.html
35. Ginestet C. ggplot2: Elegant graphics for data analysis. *J R Stat Soc A: Stat Soc*. 2011;174(1):245-246. doi:10.1111/j.1467-985X.2010.00676_9.x
36. Kolde R. pheatmap: Pretty heatmaps (1.0.13). 2025 https://cran.r-project.org/web/packages/pheatmap/index.html
37. Selma-Gonzalez J, Rubio-Guerra S, García-Castro J, et al. Association of plasma phosphorylated tau 217 with clinical deterioration across Alzheimer disease stages. *Neurology*. 2025;105(1):e213769. doi:10.1212/WNL.0000000000213769
38. Wang Y-T, Ashton NJ, Therriault J, et al. Identify biological Alzheimer's disease using a novel nucleic acid–linked protein immunoassay. *Brain Commun*. 2025;7(1):fcaf004. doi:10.1093/braincomms/fcaf004
39. Jiang Y, Zhou X, Ip FC, et al. Large-scale plasma proteomic profiling identifies a high-performance biomarker panel for Alzheimer's disease screening and staging. *Alzheimer's Dement*. 2022;18(1):88-102. doi:10.1002/alz.12369
40. Jiang Y, Uhm H, Ip FC, et al. A blood-based multi-pathway biomarker assay for early detection and staging of Alzheimer's disease across ethnic groups. *Alzheimer's Dement*. 2024;20(3):2000-2015. doi:10.1002/alz.13676
41. Planche V, Manjon JV, Mansencal B, et al. Structural progression of Alzheimer's disease over decades: The MRI staging scheme. *Brain Commun*. 2022;4(3):fcac109. doi:10.1093/braincomms/fcac109
42. Sims JR, Zimmer JA, Evans CD, et al.; TRAILBLAZER-ALZ 2 Investigators. Donanemab in Early Symptomatic Alzheimer Disease: The TRAILBLAZER-ALZ 2 randomized clinical trial. *JAMA*. 2023;330(6):512-527. doi:10.1001/jama.2023.13239
43. Bie Q, Jin C, Zhang B, Dong H. IL-17B: A new area of study in the IL-17 family. *Mol Immunol*. 2017;90:50-56. doi:10.1016/j.molimm.2017.07.004
44. Barata JT, Durum SK, Seddon B. Flip the coin: iL-7 and IL-7R in health and disease. *Nat Immunol*. 2019;20(12):1584-1593. doi:10.1038/s41590-019-0479-x
45. Li C, Zhao Q, Feng L, Li M. Emerging roles of adaptive immune response in Alzheimer's Disease. *Aging Dis*. 2024;16(4):2315-2342. doi:10.14336/AD.2024.0564
46. Bos I, Vos S, Verhey F, et al. Cerebrospinal fluid biomarkers of neurodegeneration, synaptic integrity, and astroglial activation across the clinical Alzheimer's disease spectrum. *Alzheimer's Dement*. 2019;15(5):644-654. doi:10.1016/j.jalz.2019.01.004
47. Chen J, Dai A-X, Tang H-L, et al. Increase of ALCAM and VCAM-1 in the plasma predicts the Alzheimer's disease. *Front Immunol*. 2023;13:1097409. doi:10.3389/fimmu.2022.1097409
48. Lee M, Lee Y, Song J, Lee J, Chang S-Y. Tissue-specific role of CX3CR1 expressing immune cells and their relationships with human disease. *Immune Netw*. 2018;18(1):e5. doi:10.4110/in.2018.18.e5
49. de la Monte SM, Tong M, Hapel AJ. Concordant and discordant cerebrospinal fluid and plasma cytokine and chemokine responses in mild cognitive impairment and early-stage Alzheimer's disease. *Biomedicines*. 2023;11(9):2394. doi:10.3390/biomedicines11092394
50. Kim T-S, Lim H-K, Lee JY, et al. Changes in the levels of plasma soluble fractalkine in patients with mild cognitive impairment and Alzheimer's disease. *Neurosci Lett*. 2008;436(2):196-200. doi:10.1016/j.neulet.2008.03.019
51. Motta M, Imbesi R, Di Rosa M, Stivala F, Malaguarnera L. Altered plasma cytokine levels in Alzheimer's disease: Correlation with the disease progression. *Immunol Lett*. 2007;114(1):46-51. doi:10.1016/j.imlet.2007.09.002
52. Eldjarn GH, Ferkingstad E, Lund SH, et al. Large-scale plasma proteomics comparisons through genetics and disease associations. *Nature*. 2023;622(7982):348-358. doi:10.1038/s41586-023-06563-x

53. Heo G, Xu Y, Wang E, et al. Large-scale plasma proteomic profiling unveils diagnostic biomarkers and pathways for Alzheimer's disease. *Nat Aging*. 2025;5(6):1114-1131. doi:10.1038/s43587-025-00872-8
54. Commissioner, O. of the. *FDA Clears First Blood Test Used in Diagnosing Alzheimer's Disease*. FDA; 2025. https://www.fda.gov/news-events/press-announcements/fda-clears-first-blood-test-used-diagnosing-alzheimers-disease
55. Mundada NS, Rojas JC, Vandevrede L, et al. Head-to-head comparison between plasma p-tau217 and flortaucipir-PET in amyloid-positive patients with cognitive impairment. *Alzheimer's Res Ther*. 2023;15(1):157. doi:10.1186/s13195-023-01302-w
56. Teunissen CE, Kolster R, Triana-Baltzer G, Janelidze S, Zetterberg H, Kolb HC. Plasma p-tau immunoassays in clinical research for Alzheimer's disease. *Alzheimer's Dement*. 2025;21(1):e14397. doi:10.1002/alz.14397
57. Feizpour A, Doecke JD, Doré V, et al. Detection and staging of Alzheimer's disease by plasma p-tau217 on a high throughput immunoassay platform. *eBioMedicine*. 2024:109:105405. doi:10.1016/j.ebiom.2024.105405
58. Rickenbach C, Mallone A, Häusle L, et al. Altered T-cell reactivity in the early stages of Alzheimer's disease. *Brain*. 2025:awaf167. doi:10.1093/brain/awaf167
59. Asadi MR, Gharesouran J, Sabaie H, et al. Neurotrophin growth factors and their receptors as promising blood biomarkers for Alzheimer's Disease: A gene expression analysis study. *Mol Biol Rep*. 2024;51(1):49. doi:10.1007/s11033-023-08959-4
60. Yang H-S, Yau W-YW, Carlyle BC, et al. Plasma VEGFA and PGF impact longitudinal tau and cognition in preclinical Alzheimer's disease. *Brain*. 2024;147(6):2158-2168. doi:10.1093/brain/awae034
61. Boumali R, Urli L, Naim M, et al. Kallikrein-related peptidase's significance in Alzheimer's disease pathogenesis: A comprehensive survey. *Biochimie*. 2024;226:77-90. doi:10.1016/j.biochi.2024.04.001
62. Park J-C, Jung KS, Kim J, et al. Performance of the QPLEXTM Alz plus assay, a novel multiplex kit for screening cerebral amyloid deposition. *Alzheimers Res Ther*. 2020;13(1):12. doi:10.21203/rs.3.rs-37991/v2. Research Square.
63. The AHEAD 3-45 study: Design of a prevention trial for Alzheimer's disease—Rafii - 2023 - Alzheimer's & Dementia—Wiley Online Library. (n.d.). Retrieved June 13, 2025, from https://alz-journals.onlinelibrary.wiley.com/doi/full/10.1002/alz.12748
64. Wang Z, Chen Y, Gong K, et al. Cerebrospinal fluid proteomics identification of biomarkers for amyloid and tau PET stages. *Cell Rep Med*. 2025;6(4):102031. doi:10.1016/j.xcrm.2025.102031
65. Shokrpour S, MoghadamFarid A, Bazzaz Abkenar S, Haghi Kashani M, Akbari M, Sarvizadeh M. Machine learning for Parkinson's disease: A comprehensive review of datasets, algorithms, and challenges. *Npj Parkinson's Dis*. 2025;11(1):187. doi:10.1038/s41531-025-01025-9
66. Caron NS, Haqqani AS, Sandhu A, et al. Cerebrospinal fluid biomarkers for assessing Huntington disease onset and severity. *Brain Commun*. 2022;4(6):fcac309. doi:10.1093/braincomms/fcac309
67. Yates LA, Aandahl Z, Richards SA, Brook BW. Cross validation for model selection: A review with examples from ecology. *Ecol Monogr*. 2023;93(1):e1557. doi:10.1002/ecm.1557
68. DeGroat W, Mendhe D, Bhusari A, Abdelhalim H, Zeeshan S, Ahmed Z. IntelliGenes: A novel machine learning pipeline for biomarker discovery and predictive analysis using multi-genomic profiles. *Bioinformatics*. 2023;39(12):btad755. doi:10.1093/bioinformatics/btad755
69. Ileri K. Comparative analysis of CatBoost, LightGBM, XGBoost, RF, and DT methods optimised with PSO to estimate the number of k-barriers for intrusion detection in wireless sensor networks. *Int J Mach Learn Cybern*. 2025;16:6937–6956. doi:10.1007/s13042-025-02654-5
70. Freijeiro-González L, Febrero-Bande M, González-Manteiga W. A critical review of LASSO and Its derivatives for variable selection under dependence among covariates. *Int Stat Rev*. 2022;90(1):118-145. doi:10.1111/insr.12469

SUPPORTING INFORMATION

Additional supporting information can be found online in the Supporting Information section at the end of this article.

How to cite this article: Zheng W, Jiang Y, Wong HY, et al. Targeted blood proteome profiling using NULISAseq identifies a high-performance biomarker panel for Aβ pathology quantification and staging. *Alzheimer's Dement*. 2026;22:e71179. https://doi.org/10.1002/alz.71179